© 2016. Published by The Company of Biologists Ltd | Journal of Cell Science (2016) 129, 1512-1522 doi:10.1242/jcs.176685

TOOLS AND TECHNIQUES

Tailored placement of a turn-forming PA tag into the structured domain of a protein to probe its conformational state

Yuki Fujii[1,2], Yukiko Matsunaga[1], Takao Arimori[1], Yu Kitago[1], Satoshi Ogasawara[2], Mika K. Kaneko[2], Yukinari Kato[2] and Junichi Takagi[1,*]

ABSTRACT

Placement of a tag sequence is usually limited to either terminal end of the target protein, reducing the potential of epitope tags for various labeling applications. The PA tag is a dodecapeptide (GVAMPGAEDDVV) that is recognized by a high-affinity antibody NZ-1. We determined the crystal structure of the PA-tag–NZ-1 complex and found that NZ-1 recognizes a central segment of the PA tag peptide in a tight β-turn configuration, suggesting that it is compatible with the insertion into a loop. This possibility was tested and confirmed using multiple integrin subunits and semaphorin. More specifically, the PA tag can be inserted at multiple locations within the integrin α_{IIb} subunit (encoded by *ITGA2B*) of the fibrinogen receptor $\alpha_{IIb}\beta_3$ integrin (of which the β_3 subunit is encoded by *ITGB3*) without affecting the structural and functional integrity, while maintaining its high affinity for NZ-1. The large choice of the sites for 'epitope grafting' enabled the placement of the PA tag at a location whose accessibility is modulated during the biological action of the receptor. Thus, we succeeded in converting a general anti-tag antibody into a special anti-integrin antibody that can be classified as a ligand-induced binding site antibody.

KEY WORDS: Epitope tag, Integrin, Site-specific labeling, β-turn, Reporter antibody

INTRODUCTION

Monoclonal antibodies show exquisite specificity toward their respective antigen by displaying a binding pocket with high chemical and geometrical complementarity to the antigen surface. The pocket is lined by a set of spatially arranged residues in the complementarity-determining region (CDR) loops of the antibody variable region. On the antigen, the epitope residues also need to be correctly arranged in three dimensions, rather than just being closely positioned in a primary sequence. As the conformation of a peptide segment in the structured protein is usually very different from that of free oligopeptide with the same sequence in solution (Dyson et al., 1988), it can be difficult to obtain monoclonal antibodies that are capable of recognizing native protein with high affinity by using a synthetic linear peptide as the immunizing or screening antigen (Spangler, 1991). For antibodies raised against small peptide fragments of proteins in order to generate reactivity with the cognate sequence of the intact protein, it is generally believed that they have to be targeted to highly mobile segments (Tainer et al., 1984). However, anti-peptide monoclonal antibodies are indifferent from other anti-protein monoclonal antibodies in their requirement for correct three-dimensional (3D) arrangement of epitope residues, other than the fact that all crucial residues are provided from a single stretch of primary sequence. Meanwhile, numerous monoclonal antibodies recognizing short linear peptide with high affinity and/or specificity have been successfully obtained. Some such peptide and anti-peptide monoclonal antibody pairs have been incorporated into research tools collectively called 'epitope tag system', with which one can detect, label, capture and even purify tagged target proteins very easily (Wood, 2014). Use of such a system is vital to much biomedical research, especially when good antibodies against the target molecule are unavailable.

In addition to the utility as an immunological detection agent, monoclonal antibodies can sometimes be used as probe or reporter for certain functional states of a protein, particularly when the protein undergoes a large conformational change during its biological action (Dennison et al., 2014; Humphries et al., 2003; Irannejad et al., 2013; Walker et al., 2004). If the 3D structure of the protein is known, it is theoretically possible to place a short peptide tag at a desired position and to use a monoclonal antibody against the tag to determine the function of the protein, as well as to modulate the function of the protein. However, this is not practically possible because the tag insertion into the middle of a target protein can often destroy its local conformation or alter its function. For this reason, affinity tags are fused to either the N- or C-terminus of a target protein in most applications. Even when the tag sequence insertion is not expected to affect the function of target protein, such attempts are rare, because the inserted peptide itself does not usually work as a tag any more owing to the limited accessibility of the antibody and/or the altered conformation of the tag. However, we sometimes come across cases where protein termini are important for the function, or are buried and not accessible to a binding molecule or agent, in which case we have to seek ways to attach tags somewhere else. There are several studies reporting successful insertion of tag sequence into the middle of a protein domain by targeting a flexible loop region that does not have secondary structure. In these reports, however, either very long loops were chosen as the insertion point (Dinculescu et al., 2002; Morlacchi et al., 2012; Smith et al., 2004) or the inserted tag was flanked by long linker sequences (Facey and Kuhn, 2003; Kendall and Senogles, 2006), limiting general applicability of this approach. Therefore, there are unmet needs for the development of a general tagging system that is compatible with the insertion or 'grafting' into a structured protein domain for various cell biology and biochemical applications.

Recently, we have reported the successful construction of a novel epitope tag system, by combining a 12-residue peptide (PA tag) derived from human podoplanin and a high affinity monoclonal antibody (NZ-1) against it (Fujii et al., 2014). The binding affinity

[1]Laboratory of Protein Synthesis and Expression, Institute for Protein Research, Osaka University, 3-2 Yamadaoka, Suita, Osaka 565-0871, Japan. [2]Department of Regional Innovation, Tohoku University Graduate School of Medicine, 2-1 Seiryo-machi, Aoba-ku, Sendai 980-8575, Japan.

*Author for correspondence (takagi@protein.osaka-u.ac.jp)

Received 29 June 2015; Accepted 10 February 2016

Journal of Cell Science

Journal of Cell Science (2016) 129, 1512-1522 doi:10.1242/jcs.176685

of NZ-1 toward its epitope peptide is one to two orders of magnitude higher than that of other popular anti-tag monoclonal antibodies, including the anti-FLAG M2 antibody. We found that the NZ-1–PA-tag system, which has been made available from commercial source, can be applied to a wide variety of applications, including western blotting, immunoprecipitation and immunoaffinity purification. Particularly important is its compatibility with purification, where low-abundance proteins present in cell culture supernatants or in cell lysates can be purified to near homogeneity in just one step. Detailed binding analysis has revealed that NZ-1 recognizes the core central portion of the PA tag, independently of the sequence or structure of the peptides flanking both sides. This property encouraged us to investigate the possibility of using the PA tag system in the 'epitope grafting' application.

In this study, we determined the crystal structure of the NZ-1–PA-tag complex and found that NZ-1 recognizes a β-turn structure that is formed at the center of the PA peptide. The structure indicates that the PA tag is compatible with the insertion into exposed loops without accompanying linker sequences, which was experimentally confirmed in multiple target proteins. Furthermore, insertion of the PA tag in a pinpointed manner enabled tailored placement of the NZ-1 epitope into the α_{IIb} integrin subunit (encoded by *ITG2AB*) of a platelet fibrinogen receptor, $\alpha_{IIb}\beta_3$ integrin (where the β_3 subunit is encoded by *ITGB3*), as well as into the mouse β_1 integrin, transforming a general anti-tag monoclonal antibody into a specialized reporter and/or activator antibody that can be classified as a ligand-induced binding site (LIBS) antibody.

RESULTS

Structure of the NZ-1 Fab in complex with the PA tag peptide

The NZ-1 fragment antigen-binding (Fab) fragment was crystallized either in the presence of an excess concentration of a 14-residue PA (PA14) peptide (EG**GVAMPGAEDDVV**, residues in bold correspond to the PA tag sequence) or on its own, leading to the determination of high-resolution structures of the complex (1.70 Å) and of the apo form (1.65 Å), respectively (Table 1). Both crystals contained two copies of the molecules in the asymmetric unit, deriving two independent Fab structures for each form. Surprisingly, the structure of the variable (Fv) region was nearly identical, not only between two molecules in the same crystal [Cα root-mean-square deviation (RMSD) of 0.237 Å and 0.123 Å for the complex and apo form, respectively], but also between the complex and apo form (Cα RMSD < 0.466 Å) (Fig. 1A). As the structural difference between the two forms was minimal, even at the level of the conformation of the side chains involved in the direct contacts with the antigen (Fig. 1A, right), the complementarity-determining region (CDR) of NZ-1 seems to be poised at the 'binding competent' conformation, partly explaining its very high affinity. We also noted that some surface-bound H_2O molecules involved in a hydrogen bond network at the antibody–peptide interface were already immobilized in the apo form (Fig. S1), further highlighting the surface compatibility of the NZ-1 antigen-binding groove with the peptide. In the two complex structures, clear electron densities were visible for the C-terminal 11 or 12 residues of the bound PA14 peptide (Fig. 1B). Because the unseen N-terminal two residues are not contained in the regular PA tag constructs (Fujii et al., 2014), here, we have used peptide numbering based on the 12-residue PA tag peptide. The PA peptide was docked in the cleft that formed between the variable regions of the heavy and light chains (V_H and V_L, respectively) of NZ-1 (Fig. 1C), and buried ∼1200 $Å^2$ of the total solvent-accessible surface area (ASA) at the interface. As predicted, NZ-1 recognized the central region of the PA peptide, and the conformation of the region spanning residues Val2 and Val11 of the bound peptide was indistinguishable between the two molecules (Fig. 1B). Within the binding pocket of NZ-1, the PA peptide assumes a type II β-turn conformation at the 'MPGA' sequence (Fig. 1C). There are numerous contacts formed between the PA tag and NZ-1, primarily between residues 4–10 of the peptide and the NZ-1 heavy chain (Fig. 1D). Among them, the residue Met4 and Asp10 side chains provide the most prominent contribution to the interaction, consistent with the result of the surface plasmon resonance experiments using an alanine-substituted peptide reported previously (Fujii et al., 2014). Outside of the core interface, peptide residues 2, 3 and 11 also make direct or indirect hydrogen bonds with NZ-1 using their backbone, indicating that the presence of residues at these sites, but not a specific amino acid side chain, is important for the recognition.

Table 1. Data collection and refinement statistics

	Complex	apo[a]
Data collection		
Space group	$P2_1$	$P1$
Unit cell parameters	*a*=42.2 Å, *b*=80.0 Å, *c*=132.5 Å, *β*=96.5°	*a*=42.9 Å, *b*=57.2 Å, *c*=101.5 Å, *α*=97.9°, *β*=101.5°, *γ*=105.4°
Resolution [Å]	40.0–1.56 (1.65–1.56)	31.5–1.58 (1.61–1.58)
Number of unique reflections	121,358 (18,070)	118,170 (5308)
Completeness [%]	97.2 (90.2)	97.7 (89.0)
R_{sym} or R_{merge} [%][b]	5.7 (126.3)	13.0 (76.7)
Redundancy	7.5 (7.2)	6.0 (3.8)
$I/\sigma(I)$	17.5 (1.5)	24.5 (2.3)
Refinement		
Resolution range [Å]	40.0–1.56 (1.58–1.56)	31.5–1.58 (1.60–1.58)
Number of atoms		
Proteins	6404	6478
Ligands	175	0
H_2O molecules	499	610
R_{work} [%][c]	17.9 (38.1)	16.8 (27.5)
R_{free} [%][d]	21.4 (43.2)	20.4 (30.9)
RMSD bond length [Å]	0.018	0.017
RMSD bond angle [°]	1.50	1.55
RMSZ bond length	0.87	0.80
RMSZ bond angle	0.86	0.89

Values in parentheses correspond to the highest-resolution shell. RMSZ, root-mean-square value of the Z-scores.
[a]Two dataset collected from two independent crystals were merged.
[b]$R_{sym}=100\times\Sigma|I_{hkl}-\langle I_{hkl}\rangle|\Sigma\ I_{hkl}$, $\langle I_{hkl}\rangle$ is the mean value of I_{hkl}.
[c]$R_{work}=100\times\Sigma||F_o|-|F_c||/\Sigma|F_o|$. [d]$R_{free}$ was calculated from the test set (5% of the total data).

Insertion of the PA tag into loop regions of integrin and semaphorin

The unique binding mode visualized in the NZ-1–PA-peptide complex, where the tight turn of the peptide was tucked into the binding groove with both the N- and C-termini projecting away from the antibody, indicated an interesting possibility that the epitope structure could be maintained when presented as a loop within a target molecule. In order to test this hypothesis, we first tried to insert the PA tag into exposed flexible loops of two test proteins, integrin $\alpha_6\beta_1$ (the α_6 and β_1 subunits are encoded by *ITGA6* and *ITGB1*, respectively) and semaphorin 3A (Sema3A). Although the 3D structure of integrin $\alpha_6\beta_1$ is not available yet, a reasonable

Journal of Cell Science (2016) 129, 1512-1522 doi:10.1242/jcs.176685

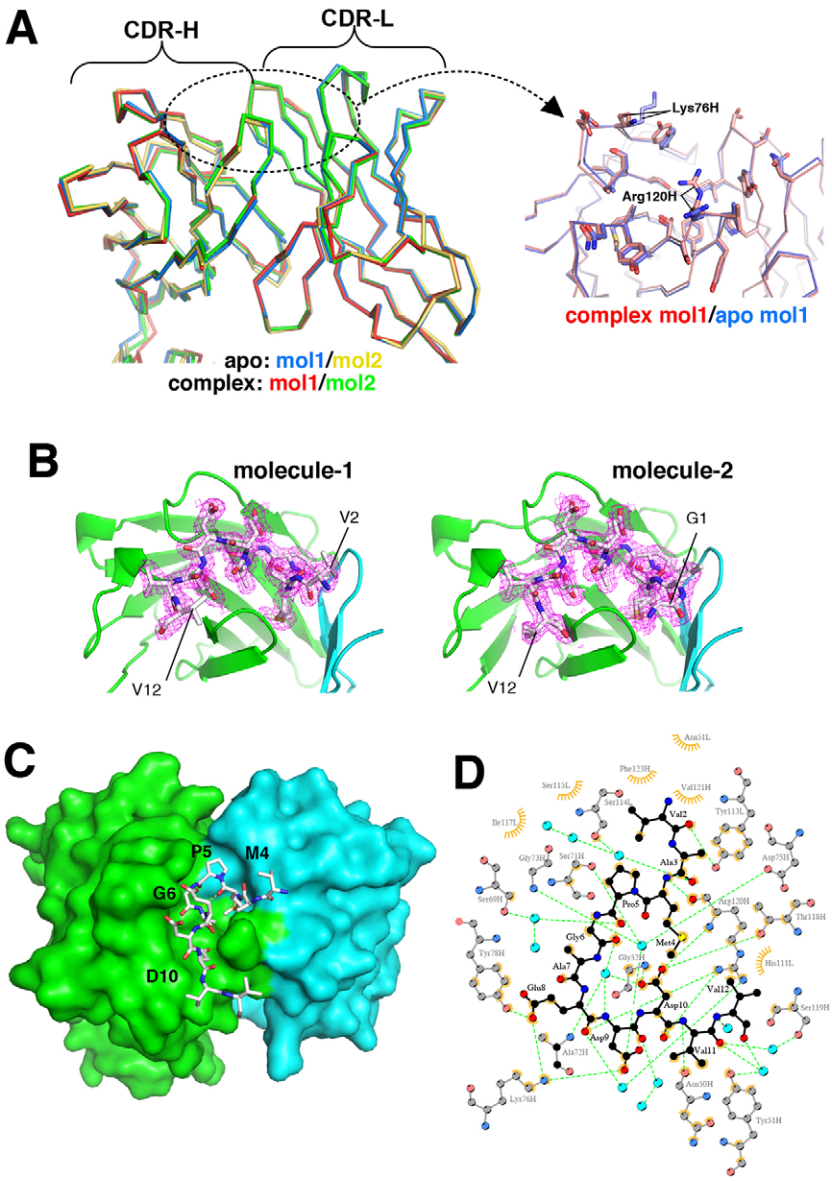

Fig. 1. Structure of the antigen-binding site of anti-PA tag antibody NZ-1. (A) Four structures of the NZ-1 Fab derived from apo and PA-tag complex forms (two molecules for each) are superposed at the Fv region and shown in C_α tracings with different colors. A close-up view of the antigen-binding pocket (dotted oval) is shown in the right, with residues that are in direct contact with the PA-tag peptide shown in the stick models. Bound peptide has been removed for clarity. CDR-H and CDR-L, CDRs of the heavy and light chains, respectively; Mol, molecule. (B) Conformation of the PA-tag peptide bound by NZ-1. Structural models for the peptide in two molecules are shown as stick model with the weighted $2F_o$-F_c electron density map (magenta wireframe) contoured at 1.0 σ. The NZ-1 Fab heavy (green) and light (cyan) chains are shown in cartoon models. (C) The PA-tag peptide (stick model) bound in the pocket on top of the NZ-1 Fab (surface model) is shown, with the main chain hydrogen bond maintaining the type II β-turn (yellow dotted line). Colors are as in B. (D) Residue-wise contacts between the NZ-1 Fab (thin colors) and the PA peptide (thick colors), analyzed by using the LIGPLOT program. The bond-length cut off was set to 3.35 Å for hydrogen bonds (denoted by green dotted line) and an inter-atomic distance range of 2.9–3.9 Å was used for van der Waals contacts (orange eyelash). Oxygen, nitrogen, carbon and water molecules are shown as red, blue, black and cyan spheres, respectively.

homology model can be built by using integrin $\alpha_5\beta_1$ (the α_5 subunit is encoded by *ITGA5*) as a template (Nagae et al., 2012). A long protruding loop predicted to be present in the thigh domain of the α_6 subunit for $\alpha_6\beta_1$ integrin (Fig. 2A) was chosen as an insertion point. For Sema3A, for which the crystal structure is known, we chose a loop in the N-terminal Sema domain (Fig. 2B). Both insertions are predicted to have no effect on the function of the respective proteins, because they are located far from the interfaces involved in the interaction with physiological binding partners (Fig. 2A,B, arrows). In fact, these mutants were expressed well at the same or even better levels than the wild-type counterparts (Fig. 2C,D, lanes 5 and 6) and exhibited normal biological activities (data not shown). Furthermore, both insertions were functionally active as epitope tags, because the secreted PA-tagged version of both proteins could be efficiently immunoprecipitated in their native state with the NZ-1 antibody from the culture medium (Fig. 2C,D, lane 2). These results clearly demonstrate that the 12-residue PA tag peptide inserted into the middle of a long flexible loop is able to assume the β-turn conformation that is required for recognition by NZ-1 and can fully function as epitope tag.

Next, we aimed to see if the PA tag could be inserted into loops with a higher degree of structural restriction. The α_{IIb} subunit of integrin $\alpha_{IIb}\beta_3$ comprises four large all-β domains and bears many surface-exposed loops that are ideal for evaluating the effect of loop length on the applicability of the PA tag insertion (Fig. 3A) (Zhu et al., 2008). First, we chose the 3-4 loop of blade 2 [referred to as W2, where a four-stranded antiparallel sheet is represented by 'W' (Springer, 1998)] of the β-propeller domain as the insertion point. As this four-residue (PESG) loop is at one end of a β-hairpin that connects neighboring strands with an end-to-end distance of only 5.2 Å (Fig. 3B), a simple insertion of the PA peptide, which has an end-to-end distance of 10.2 Å in the NZ-1-bound state, might not be structurally compatible. We therefore tested several constructs, inserting the PA tag dodecapeptide flanked by linker segments of varying lengths at the W2 site (Fig. S2A). The insertion itself did not seem to destabilize the integrin because all insertion mutants were expressed normally regardless of the linker length (Fig. S2B, lanes 8–12). Surprisingly, all these mutants could be successfully immunoprecipitated by the NZ-1 antibody (Fig. S2B, lanes 2–6), indicating that even the minimum (i.e. no

Journal of Cell Science (2016) 129, 1512-1522 doi:10.1242/jcs.176685

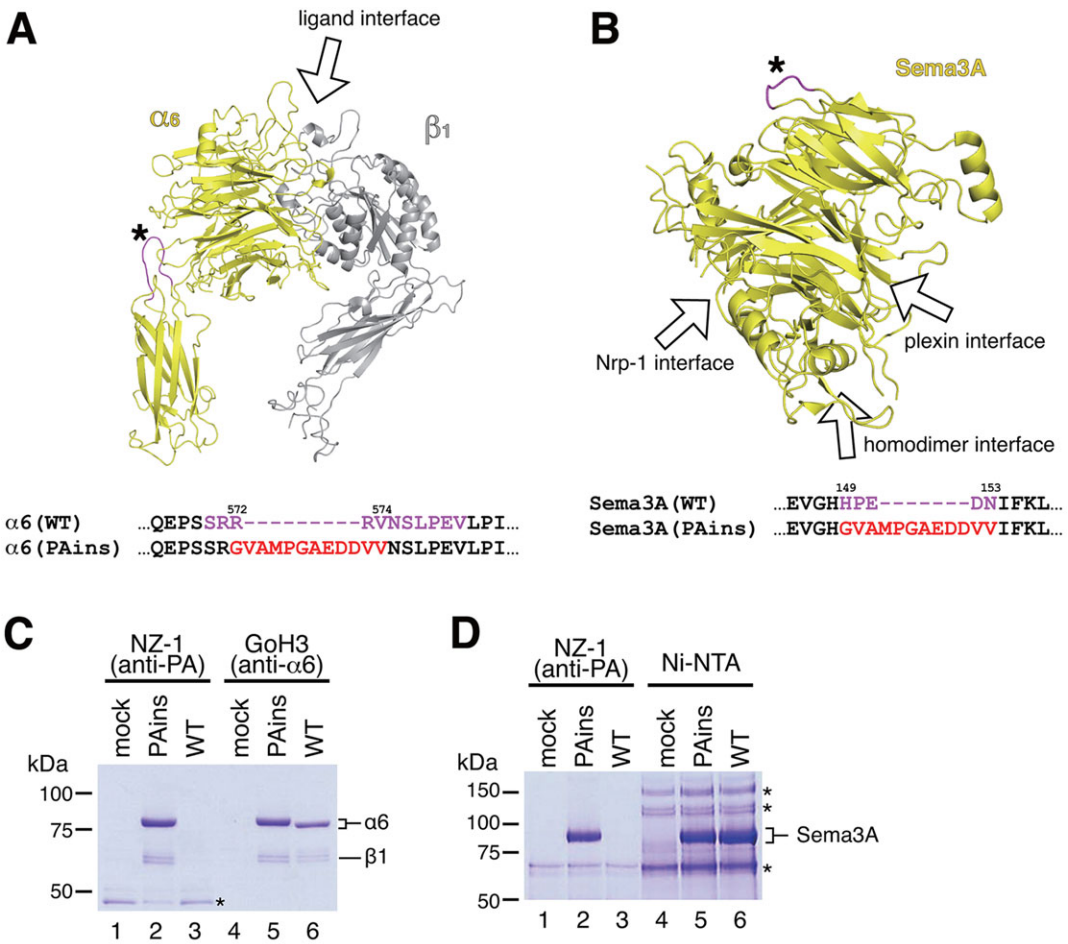

Fig. 2. The PA tag can be inserted into long flexible loops. Loops selected for the PA-tag insertion (asterisk) are shown in the homology model of the $\alpha_6\beta_1$-integrin headpiece fragment (A) and the crystal structure of mouse Sema3A (Protein Data Bank ID: 4GZ8) (B). The actual amino acid sequences for wild-type (WT) and insertion mutant (PAins) near the insertion positions are shown below the structure, with the inserted PA-tag sequence and the loop segments shown in the structure colored red and magenta, respectively. Locations of known protein–protein interfaces that are important for the function of these proteins are indicated by arrows. (C,D) Immunoprecipitation of the PA-tagged $\alpha_6\beta_1$ headpiece fragment (C, α_6+β_1) and Sema3A (D) by NZ-1. The PA-tagged, but not the WT, version of each protein could be specifically captured by NZ-1 immobilized beads and eluted by the PA peptide (lanes 2 and 3), whereas both bound to beads immobilized with anti-α_6-integrin antibody GoH3 (C, lanes 5 and 6) or to Ni-NTA agarose (D, Ni-NTA, lanes 5 and 6). Bands labeled with an asterisk were present in all samples, including that obtained from mock-transfected cells (lanes 1 and 4) and, hence, represent nonspecific contamination.

linker) PA tag inserted at a very tight hairpin loop remained reactive with NZ-1.

Next, we expanded the target location of the insertion to see if the above property of the PA tag is generally applicable. We chose nine more sites, including five β-hairpins similar to W2 (W1, cap, W3, W6, Calf1_XZ), three inter-sheet loops with intermediate lengths (Thigh_FG, Calf1_EF, Calf2_FG) and one very long loop that harbors internal furin cleavage site (Calf2_XY) (Fig. 3C; Fig. S3). First, the effect of these mutations on the structural integrity of the protein was evaluated by comparing the level of expression in the context of the soluble ectodomain fragment of the $\alpha_{IIb}\beta_3$-integrin heterodimer. As shown in Fig. 4A, all mutants except for W3 and W6 could be expressed and secreted into the medium, indicating the compatibility of these eight insertions to the native structure. The location of the W3 and W6 insertions were very close to the Ca^{2+}-binding sites known to be important for the correct folding of the β-propeller domain of α integrin subunits (Mitchell et al., 2003), suggesting that the correct metal ion coordination geometry was severely perturbed by these two mutations. Among the eight mutants that could be expressed and secreted successfully, seven were immunoprecipitated with NZ-1 at the same efficiency as that with the pan-β_3-integrin monoclonal antibody 7E3 (Fig. 4B), confirming the successful insertion and presentation of the epitope structure at a variety of locations in $\alpha_{IIb}\beta_3$ integrin. The cap mutant was reactive with NZ-1 but at a reduced level compared to that of the other constructs (Fig. 4B, lane 4). To gain a more quantitative assessment on the effect of loop insertion, we purified six $\alpha_{IIb}\beta_3$-integrin mutants and measured their binding affinity for NZ-1. Kinetic binding analyses using biolayer interferometry (BLI) derived K_D values ranging from 0.6 to 3.6 nM (Fig. 4C), which were similar to the values obtained previously with various terminally PA-tagged proteins (Fujii et al., 2014). As it is natural to expect slight variations in the affinity value of a monoclonal antibody for a peptide when the epitope is placed in different structural contexts, we conclude that insertion of the PA tag is generally applicable to a wide range of loop and turn positions in a variety of target proteins. It is also noteworthy that a functionally active PA-tag epitope can be readily inserted into the middle of a loop of target proteins without extensive optimization of linker length (Fig. S2), which has great technical advantages.

Journal of Cell Science (2016) 129, 1512-1522 doi:10.1242/jcs.176685

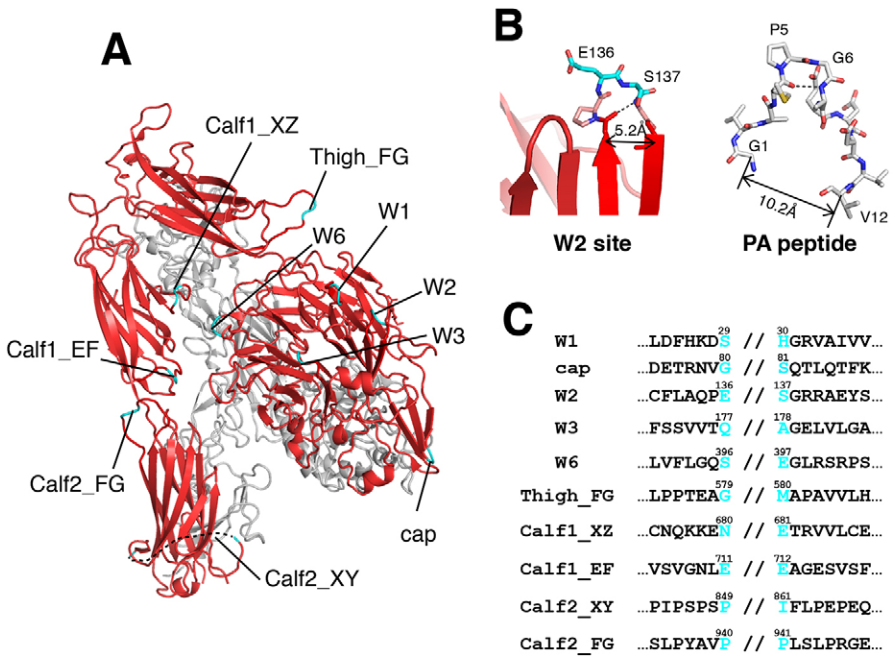

Fig. 3. Surface-exposed loops in the $\alpha_{IIb}\beta_3$-integrin ectodomain selected for the tag insertion. (A) Crystal structure of the $\alpha_{IIb}\beta_3$-integrin ectodomain (Protein Data Bank ID: 3FCS) is shown in red (α_{IIb}) and gray (β_3) cartoon models, with the ten PA-tagged loops labeled. (B) Conformation of the β-hairpin at the W2 site is shown side by side with that of the reverse U-shaped PA-tag peptide taken from the PA–NZ-1 complex structure molecule 2. (C) Amino acid sequences of the segments containing the insertion position (indicated by //).

Although we believe that the insertion compatibility of the PA tag is attributable to its turn-forming propensity revealed by the crystal structure, one could think that the compatibility merely reflects the flexible nature of the selected loops rather than reflecting a special property of the PA tag. In order to test the uniqueness of the PA tag, two popular peptide tags, Myc and FLAG, were inserted into three locations (W2, Thigh_FG and Calf1_XZ) and the functionality was compared with that of the PA tag. As evident from the successful

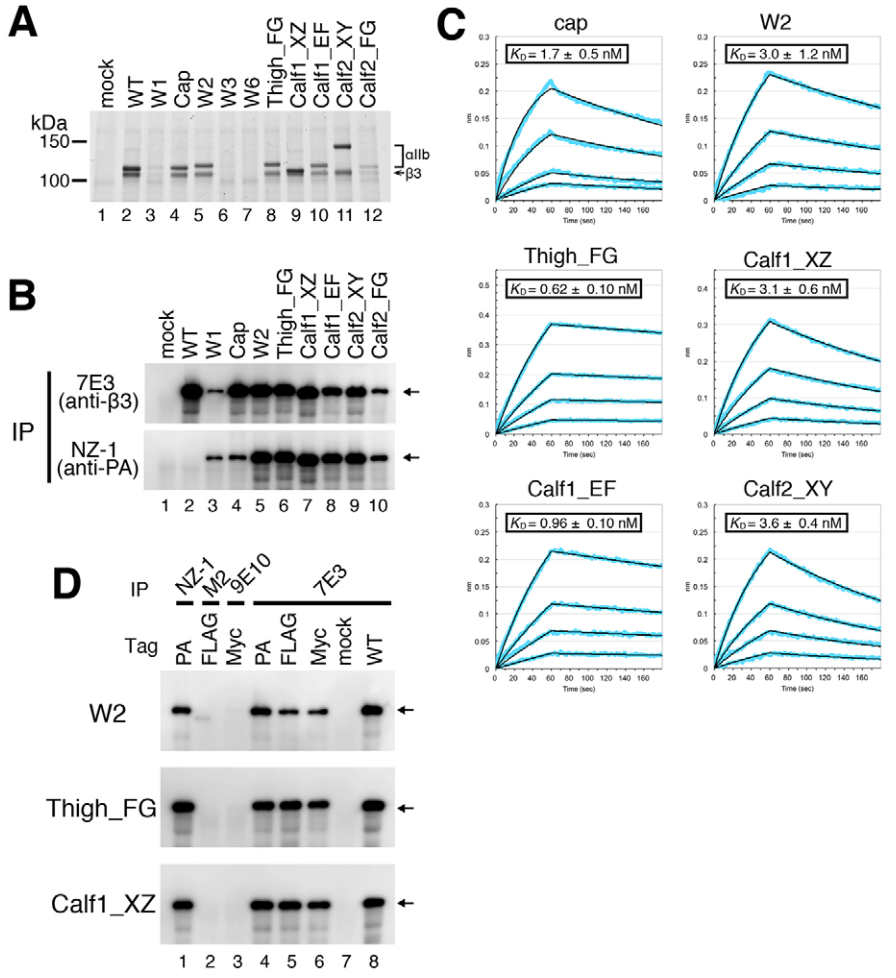

Fig. 4. The PA tag can be inserted into multiple α_{IIb}-integrin loops. (A) Soluble ectodomain fragments of integrins comprised of various α_{IIb} mutant and wild-type β_3 subunits were expressed in HEK293T cells and immunoprecipitated with the anti-velcro-tag antibody 2H11, followed by 7.5% SDS-PAGE analysis under reducing conditions and visualization with the Oriole fluorescent protein stain. Note that the mobilities of the Calf1_XZ and Calf2_XY mutant α_{IIb} chains were different from that of the wild type, owing to the elimination of an N-linked glycosylation site at residue Asn680 (for Calf1_XZ) and a furin-cleavage site within 855-KRDRR-859 (for Calf2_XY), respectively. (B) The PA-tagged mutant $\alpha_{IIb}\beta_3$ ectodomain fragments were expressed as in A and immunoprecipitated (IP) with the anti-β_3-integrin antibody 7E3 (upper panel) or NZ-1 (lower panel), followed by immunoblotting with the anti-velcro polyclonal antibody. (C) Determination of the affinity of the NZ-1 antibody toward each insertion mutant. The $\alpha_{IIb}\beta_3$-integrin ectodomain fragments with inserted PA tag were purified and subjected to kinetic binding analyses using biolayer interferometry. Each subpanel shows the overlaid binding curves obtained with four different concentrations (10, 5, 2.5 and 1.25 nM) of the PA-bearing integrin. Dissociation constant (K_D) values were derived by global curve fitting (black thin lines) to the actual binding curves (cyan) and are shown as mean±s.d. (n=3). (D) PA (lanes 1 and 4), FLAG (lanes 2 and 5) and Myc (lanes 3 and 6) tags were inserted at three select sites, immunoprecipitated with the 7E3 antibody (lanes 4–8) or corresponding anti-tag antibodies (lanes 1–3), and visualized by anti-velcro immunoblotting. In B and D, SDS-PAGE analysis was conducted under non-reducing conditions so that the $\alpha_{IIb}\beta_3$ integrin migrated as a single ~250 kDa band (arrow).

Journal of Cell Science (2016) 129, 1512-1522 doi:10.1242/jcs.176685

expression and secretion of the mutant integrins (Fig. 4D, lanes 5 and 6), insertion of these tags was structurally tolerated, as in the case of the PA tag, which is not surprising considering the shorter length of these tags (eight and ten residues for FLAG and Myc, respectively). In contrast to the PA -tagged versions, however, both inserted sequences completely lost their reactivity with their respective monoclonal antibodies (Fig. 4D, lanes 2 and 3). This result strongly suggests that Myc and FLAG sequences can no longer function as epitope tags upon presentation within these loops, underscoring the uniqueness of the PA tag.

Utility of the PA-tag–NZ-1 system to explore the conformational state of cell surface integrin

To explore the possibility of using the PA tag as a reporter system for receptor conformation, seven of the insertion mutations were introduced in the context of the cell surface $\alpha_{IIb}\beta_3$-integrin heterodimer. As judged by the flow cytometry analyses of cells stained with an antibody against α_{IIb} integrin (Fig. 5A, upper panels), all mutants were expressed well on the cell surface. The two mutants (W1 and Calf2_FG) that had exhibited decreased levels of expression and secretion in the context of the soluble ectodomain fragment (Fig. 4A) were also expressed well, suggesting that the negative effect of these insertions on the structural integrity of the receptor was not severe. More importantly, these PA-tagged integrins exhibited normal biological activity, as monitored by the activation-dependent binding of the ligand-mimetic antibody PAC-1 (Fig. 5B).

As in the case of soluble ectodomain fragments, all these PA-tagged mutant integrins were reactive with NZ-1, as judged by flow cytometry analysis (Fig. 5A, lower panels). However, we found that one mutant (Calf1_EF) showed consistently weak staining with NZ-1, in spite of its high overall expression. We reasoned that this reflects limited accessibility to the inserted PA tag in the context of cell surface integrin, because this site is predicted to be partially hidden in the 'bent' conformation of resting integrin (Fig. 6A) and previous experiments showed that the affinity of NZ-1 for this site is not particularly low compared to other mutants (Fig. 4C). In fact, NZ-1 reactivity toward this mutant was increased upon the treatment of cells with Mn^{2+} and RGD peptide, a known 'activating' condition that induces a global conformational change in integrins (Takagi et al., 2002), and such effect was not observed with two other mutants (Fig. 6B). Although the net increase in the NZ-1 reactivity was relatively small compared to the total binding signal, this assay can report a range of integrin conformational changes caused by different concentrations of soluble ligand (Fig. S4). A group of antibodies recognizing integrin whose binding is upregulated upon integrin activation or ligand-binding are called LIBS antibodies, even though the binding can be upregulated by certain cations such as Mn^{2+} in the absence of ligands. The above result clearly demonstrates that NZ-1 can behave as one of these LIBS antibodies, when combined with an appropriate PA-tag insertion design.

Cell surface integrins are known to exist in a conformational equilibrium between bent (low affinity) and extended (high affinity)

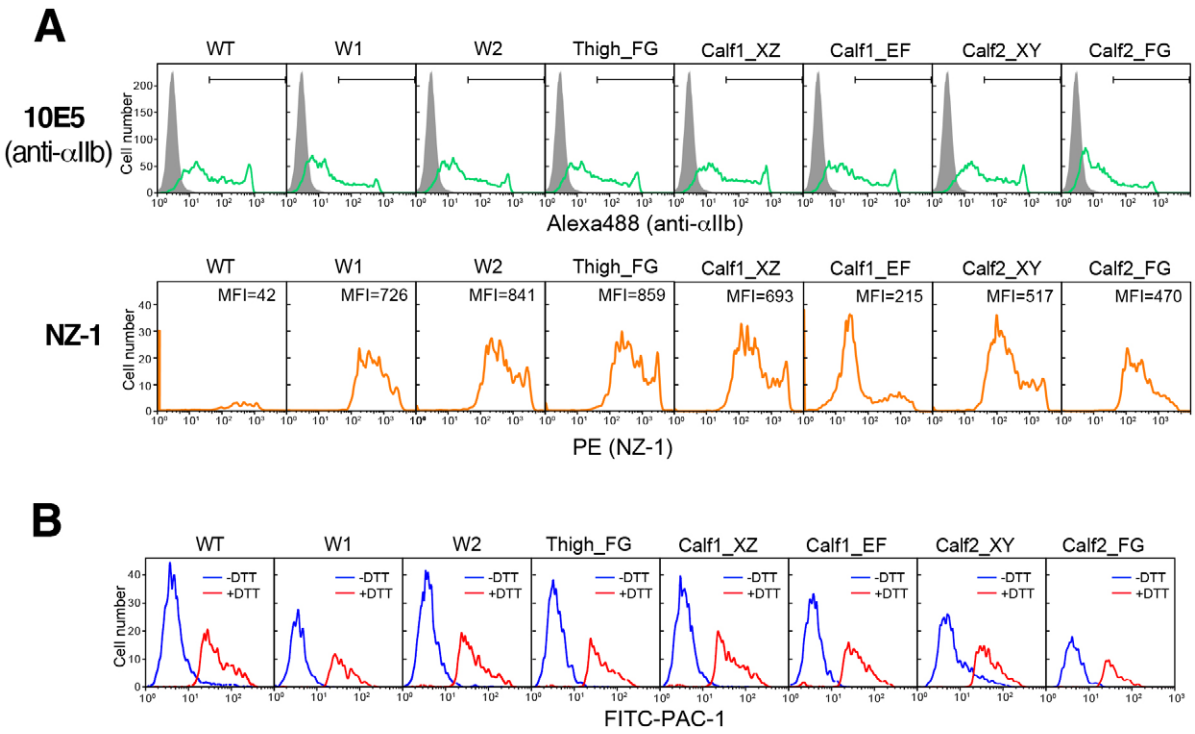

Fig. 5. Grafting the PA-tag epitope in the context of $\alpha_{IIb}\beta_3$ integrin expressed on the cell surface. (A) Various PA-tagged full-length $\alpha_{IIb}\beta_3$ integrins were transiently expressed on podoplanin-null HEK293T cells (293T-PA$^-$) and co-stained with the anti-α_{IIb}-antibody 10E5 (upper panels, green histograms) and NZ-1 (lower panels, orange histograms), followed by flow cytometry analysis using Alexa-Fluor-488- and phycoerythrin (PE)-labeled secondary antibodies against mouse and rat IgGs, respectively. Signals from untransfected parental cells (gray area in the upper panels) were used to define 10E5-positive cell populations (brackets, ~2000 cells for all mutants), and NZ-1 staining was evaluated only for those cells. The mean fluorescence intensity (MFI) values are shown. (B) Ligand-binding activity of the PA-tagged $\alpha_{IIb}\beta_3$ integrin. 293T-PA$^-$ cells that had been transiently transfected with the PA-tagged $\alpha_{IIb}\beta_3$ integrin were left untreated (blue solid line) or incubated with DTT (red solid line) to activate the integrin and were then co-stained with Dylight680–AP3 (pan-β_3-integrin monoclonal antibody) and FITC–PAC-1. The histograms show the FITC fluorescence (i.e. PAC-1 binding) from the cell populations that were positive for AP3 staining. WT, wild-type $\alpha_{IIb}\beta_3$-integrin construct.

Journal of Cell Science (2016) 129, 1512-1522 doi:10.1242/jcs.176685

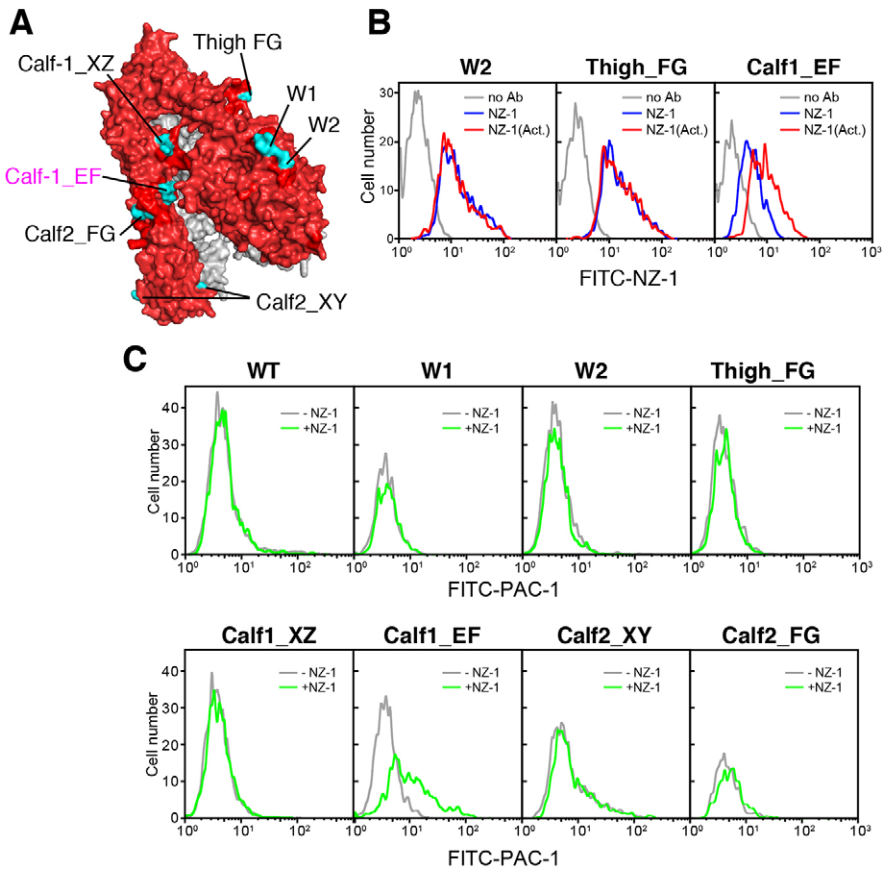

Fig. 6. The 'LIBS' nature of the PA tag inserted at the Calf1_EF site. (A) Location of the loop insertion. The entire $\alpha_{IIb}\beta_3$-integrin ectodomain in the bent form (Protein Data Bank ID: 3FCS) is shown as a surface model, with α_{IIb}-integrin and β_3-integrin chains in red and gray, respectively. Locations of PA-tag insertions into loops used in the experiments are highlighted in cyan and labeled. Note that the Calf1_EF site is located inside the bend, partially occluded by the bowed head, comprising the β-propeller domain. (B) Conformation-dependent epitope exposure. 293T-PA$^-$ cells that transiently expressed $\alpha_{IIb}\beta_3$-integrin with the three different PA-tag insertions indicated were incubated with Dylight680–AP3 alone (gray), Dylight680–AP3 and FITC–NZ-1 (blue), or Dylight680–AP3, FITC–NZ-1, 0.5 mM $MnCl_2$ and 1 mM RGD peptide (red). FITC fluorescence histograms obtained with AP3-positive cell populations are shown. (C) The ligand-binding activity of $\alpha_{IIb}\beta_3$-integrin with the Calf1_EF mutation can be activated by NZ-1. 293T-PA$^-$ cells that had been transiently transfected with the PA-tagged $\alpha_{IIb}\beta_3$-integrin were stained with Dylight680–AP3 and FITC–PAC-1 in the absence (gray) or presence (green) of 10 µg/ml unlabeled NZ-1. FITC fluorescence histograms from the cell populations that were positive for AP3 staining are shown. WT, wild-type $\alpha_{IIb}\beta_3$-integrin construct.

states, and shifting this equilibrium from inside the cell constitutes the regulatory mechanism of cell adhesion (Carman and Springer, 2003). Because exogenous addition of antibodies that preferentially bind to the extended conformation (such as LIBS monoclonal antibodies) can generally shift the equilibrium toward the high-affinity state, they can often 'activate' integrins from outside of the cell (Humphries, 2004). On the resting cell surface, wild-type $\alpha_{IIb}\beta_3$ integrin exhibited negligible binding of the PAC-1 ligand, regardless of the addition of NZ-1 (Fig. 6C, panel WT). However, the cells expressing the Calf1_EF mutant of $\alpha_{IIb}\beta_3$ integrin specifically bound to ligand upon addition of a saturating concentration of NZ-1. This effect was not observed in other PA-tagged mutants, indicating that the increased ligand binding was due to the conformational change of integrin induced by NZ-1 and not by the bound NZ-1 itself.

Encouraged by the successful conversion of NZ-1 into a LIBS antibody for human $\alpha_{IIb}\beta_3$ integrin as described above, we next designed an 'activation reporter' mutant for a different integrin subunit. As most integrin LIBS antibodies available are specific for human integrins, development of antibodies that can report conformational changes of mouse integrin is of great value. The HUTS-4 mouse monoclonal antibody against human β_1 integrin is an activation-reporter antibody whose epitope residues have been precisely defined (Mould et al., 2003). We inserted the PA tag at the E-F loop of the mouse β_1 hybrid domain that harbors Asn417, which corresponds to the HUTS-4 epitope in human β_1 integrin (Fig. 7A). When transiently transfected into HEK293T cells together with the human α_4-integrin subunit, the PA-tagged mouse β_1 integrin was expressed well on the cell surface and it could be stained with NZ-1 (Fig. 7Bi, blue). When the cells were treated with 1 mM $MnCl_2$, a condition known to expose the activation epitope on β_1 integrin (Takagi et al., 1997), the NZ-1 reactivity was upregulated, as expected (Fig. 7Bi, red). A rat monoclonal antibody recognizing β_1 integrin (9EG7), a known LIBS antibody that can recognize both human and mouse β_1-integrin chains (Bazzoni et al., 1995), also showed increased binding upon Mn^{2+} treatment (Fig. 7Bii). However, the magnitude of the epitope exposure over a range of Mn^{2+} concentrations was greater for NZ-1 than for 9EG7 (Fig. 7C), although the total maximum binding sites per cells should be higher for 9EG7 because of the simultaneous recognition of transfected mouse β_1-integrin and endogenous human β_1-integrin chains. Therefore, the combination of the PA-tagged β_1 integrin and NZ-1 offers a unique opportunity for the conformational probing of β_1 integrins in various cell biology applications.

DISCUSSION

As a result of the structural analysis of the NZ-1–PA-peptide complex, basis for the high affinity and specificity of this interaction was justified. First, comparison between the structure of the apo state (i.e. without peptide) and the complex revealed that only a minimal change is required for the unbound NZ-1 to accommodate the PA-tag peptide, providing a structural basis for the very high affinity. Another potential source for the high affinity likely resides in the β-turn-forming propensity of the peptide. Because the Pro-Gly sequence is known to occur very frequently in the type-II turn of known protein structures (Guruprasad and Rajkumar, 2000), this part of the epitope structure tends to be 'preformed', before the encounter with NZ-1, making the binding entropically favorable. We discovered, however, that this turn-forming propensity of the PA tag has a far more important implication in its unique utility in the 'loop insertion' application. Inserting a functional tag sequence into a protein has been difficult because the inserted tag would have difficulty in assuming the correct conformation for the antibody

Journal of Cell Science (2016) 129, 1512-1522 doi:10.1242/jcs.176685

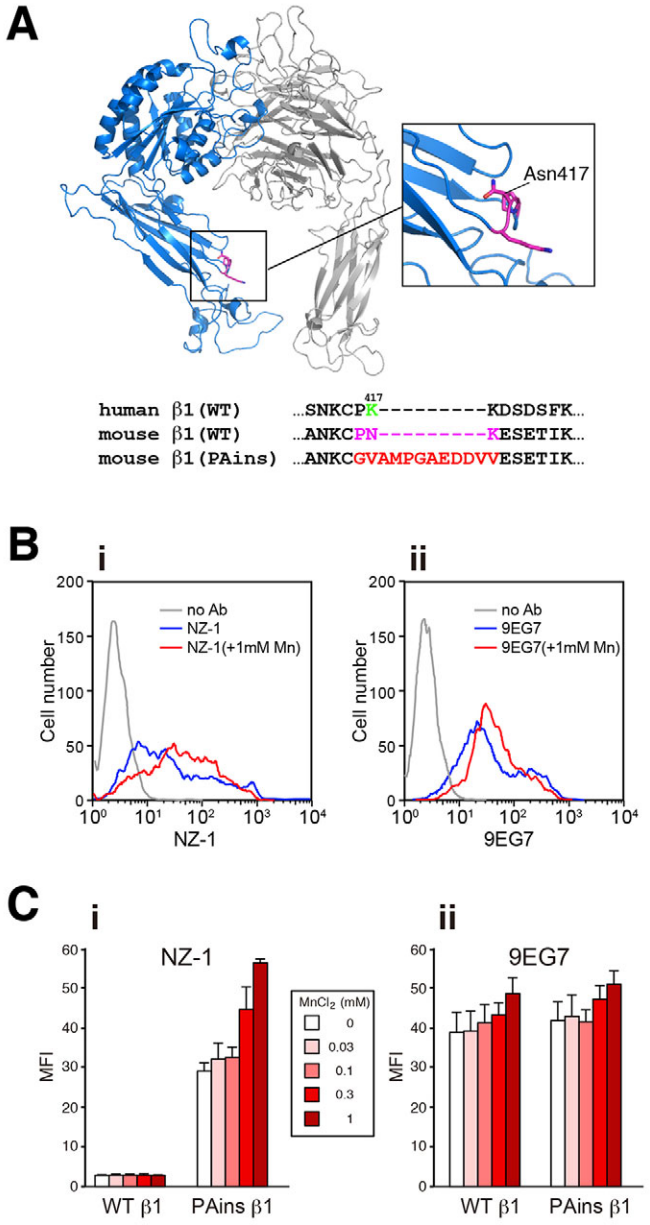

Fig. 7. Targeted insertion of the PA tag at a 'LIBS' site in the mouse β_1 integrin. (A) A homology model of the headpiece portion of mouse β_1 integrin (blue) in complex with the human α_4-integrin chain (gray) is shown in a ribbon model, with the three-residue portion replaced by the PA tag sequence in the designed mutant (PAins) shown in magenta with a stick model. Residue Asn417 at the center of this segment (inset) corresponds to one of the crucial epitope residues (Lys417) for the LIBS monoclonal antibody HUTS-4 in human β_1 integrin. Sequence alignment of human and mouse β_1 integrin near the insertion site is shown at the bottom of the panel. (B) Flow cytometry profiles of NZ-1 (i) or 9EG7 (ii) binding to 293T-PA$^-$ cells expressing mouse β_1-integrin (PAins) in the absence (blue) or presence (red) of 1 mM $MnCl_2$. (C) The binding of NZ-1 (i) or 9EG7 (ii) to either wild-type (WT) or PAins mutant versions of mouse β_1 integrin were evaluated as described in B in the presence of varying concentrations of $MnCl_2$. The data are presented as the mean fluorescence intensity (MFI) of the total cell population. Data are mean±s.d. from three independent experiments.

binding owing to the structural constraints. Certain high-affinity antibodies against linear tag peptides recognize relatively long stretches of peptide in an extended conformation (Krauss et al., 2008), which is difficult to achieve when inserted into a folded protein domain. In contrast, NZ-1 recognizes the central region of the PA tag when the tag is in a compact folded configuration, enabling the presentation of a functional epitope structure in a loop of a folded globular domain. Furthermore, the PA tag can be inserted into a very tight hairpin without a need for extensive optimization or addition of linker residues. So far, we have successfully grafted the PA tag onto several different targets, including α_6-integrin, α_{IIb}-integrin and β_1-integrin chains, as well as into Sema3A (Figs 2, 3 and 7). Our ongoing research also suggests that the tag can be inserted into surface-exposed loops of multi-pass membrane proteins without compromising their biological functions (data not shown). Precise structural information regarding the target protein is helpful but not essential for design of the insertion site, as long as one can build a reasonable homology model with the correct secondary structure assignments for the target.

The 'insertion' compatibility of the PA-tag system provides several benefits that have been lacking with other epitope tag systems. First, it can offer a way to attach purification tags to targets whose N- and C-termini are not available for functional or structural reasons. These include cases where termini are inaccessible to antibody in the native structure or cannot be modified because they are an integral part of the active site of the target protein. Second, the utility of the inserted tag is not limited to the purification purpose. Because one can insert the PA tag into a desired location of the target molecule in a pinpointed manner, it offers an easy way to achieve site-specific labeling in many applications. Third, the PA tag (12 residues) is substantially smaller than GFP or other insertion-compatible protein domains and, hence, less likely to cause structural and functional alterations. Finally, owing to the very slow dissociation rate of the PA-tag–NZ-1 interaction (Fujii et al., 2014), labeling with the Fab or the single chain variable fragment (scFv) of NZ-1 could be used to visualize individual domains or subunits in electron microscopy analyses or to probe conformational dynamics in Förster resonance energy transfer (FRET) experiments.

The advantage of the site-specific PA-tag insertion can also be appreciated in a unique application where a general anti-tag monoclonal antibody is converted into a conformation reporter or modulator, as exemplified by the results with the α_{IIb} and β_1 integrins presented here. Integrin experimental biology has greatly benefitted from the use of various conformation-dependent monoclonal antibodies. Numerous studies have identified so-called LIBS antibodies, which preferentially recognize activated or high-affinity state integrin conformations (Humphries, 2004), leading to the concept that the conformationally polymorphic integrin undergoes global extension to expose LIBS epitopes during activation and ligand binding (Takagi and Springer, 2002). However, such monoclonal antibodies are obtained by chance, and LIBS antibodies are available for only a limited set of integrin subunits. Particularly, LIBS antibodies that can react with mouse integrins are in short supply, because most monoclonal antibodies are still produced in mice. Another problem with the currently available LIBS monoclonal antibodies is that it is impossible to perform quantitative comparisons between the patterns of epitope exposure (i.e. conformational change) by using multiple antibodies against different epitopes because of the inevitable difference in their binding affinity and kinetics. In contrast, NZ-1 would bind to the grafted PA epitope with similar binding affinity regardless of the location of the insertion (Fig. 4C). Therefore, the PA-tag–NZ-1 system will provide an opportunity not only to detect conformational changes of integrins that have been previously difficult to detect owing to the lack of appropriate antibody, but also to gain insights into the real conformational dynamics of cell surface

Journal of Cell Science (2016) 129, 1512-1522 doi:10.1242/jcs.176685

integrins by allowing comparative analysis of the exposure kinetics for different epitopes. For applications involving cell-based assays, one must avoid using human cells that express endogenous podoplanin, the original antigen for the NZ-1 monoclonal antibody. In order to get around this problem, we have established a HEK293T-derived cell line devoid of podoplanin expression (293T-PA^{-}), which can be provided upon request. Moreover, NZ-1 does not react with podoplanin of mouse, rat, hamster or dog origin (Fujii et al., 2014), and is fully compatible with cells from these animals. Therefore, the uses described above are not limited to integrin research and should be applicable to studies of any signaling system that involves receptor conformational change.

Another yet unexplored possibility of the PA-tag–NZ-1 system is its use as a tool for facilitating crystallization. Crystallization chaperones are attracting much attention as a promising way to increase the likelihood of obtaining well-ordered crystals of biologically important and difficult targets for structural studies (Koide, 2009). The advantages of chaperone-mediated crystallization are thought to be twofold: firstly, it can reduce conformational heterogeneity of target molecules by binding to a specific conformation, and secondly can provide increased surface area to promote crystal lattice formation (Koide, 2009). Monoclonal antibodies are ideal candidates as crystallization chaperones, but they have to be individually developed and screened for each target, making the strategy very costly and unpredictable. The idea of developing a portable peptide tag and anti-tag 'chaperoning' antibody has been pursued by Lieberman and colleagues (Johnson et al., 2015), but the technology has not been realized so far. As the inserted PA tag is a 'foreign' structure placed on the client protein, NZ-1 might not have a strong stabilizing effect on the conformation, as in the case of the target-specific chaperone antibody. If the inserted loop is sufficiently short, however, the bound NZ-1 will have minimum mobility while presenting sufficient surface for the lattice contacts. Therefore, use of NZ-1 Fab in assisting crystallization, particularly for multi-pass membrane proteins where the PA tag is inserted into one of extramembranous loops, might prove highly promising, and further studies are eagerly awaited.

MATERIALS AND METHODS

Antibodies and peptide

The monoclonal antibodies used in this study were: 2H11 (anti-ACID/BASE 'velcro', kindly provided by Ellis Reinherz) (Chang et al., 1994), AP3 (anti-β_3 integrin, HB-242, obtained from American Type Culture Collection) (Newman et al., 1985), 7E3 (anti-β_3-integrin, kindly provided by Barry S. Coller) (Coller, 1985), 10E5 (anti-α_{IIb}-integrin, kindly provided by B. S. Coller) (Peerschke and Coller, 1984), GoH3 (anti-α_6-integrin, MAB1378, Merck Millipore), 9EG7 (anti-β_1-integrin, 553715, BD Biosciences) (Bazzoni et al., 1995), M2 (anti-FLAG, F-3165, Sigma-Aldrich) and 9E10 (anti-Myc, 017-21871, Wako Pure Chemical Industries, Ltd.). Anti-PA tag rat monoclonal antibody NZ-1 IgG was either purified from hybridoma culture supernatants (Fujii et al., 2014) or purchased from Wako Pure Chemical Industries, Ltd. (016-25861). The rabbit anti-velcro polyclonal antibody (Takagi et al., 2001) was biotinylated using EZ-link Sulfo-NHS-LC-Biotin (Thermo Scientific). Fluorescent labeling of AP3 was conducted using DyLight 680 NHS Ester (Thermo Scientific) according to the manufacturer's recommendation. The FITC-conjugated mouse anti-$\alpha_{IIb}\beta_3$ ligand-mimetic antibody PAC-1 (FITC–PAC-1) was obtained from Becton, Dickinson and Co. (340507). The Alexa-Fluor-488-conjugated goat anti-mouse IgG polyclonal antibody (rat absorbed) and the phycoerythrin-conjugated goat anti-rat IgG polyclonal antibody (mouse absorbed) were obtained from Invitrogen (A11029) and Southern Biotechnology (3010-09), respectively. The PA14 peptide (EGGVAMPGAEDDVV) was synthesized and purified as described previously (Fujii et al., 2014), and RGD peptide (GRGDSPK) was purchased from Sigma-Aldrich.

Preparation of NZ-1 Fab

Purified NZ-1 IgG was dialyzed against PE buffer (20 mM sodium and potassium phosphate, 10 mM EDTA, pH 7.0) and incubated with immobilized papain (Thermo Scientific) (0.1 ml per mg of IgG) in the presence of 25 mM cysteine-HCl (pH 7.0) for ∼4 h at 37°C under gentle agitation. After the removal of the immobilized papain, the reaction mixture was dialyzed against Tris-buffered saline (TBS; 50 mM Tris-HCl, 150 mM NaCl, pH 7.5) and slowly added to PA14-peptide-conjugated Sepharose. Bound Fab was eluted with 10 mM MES containing 3 M $MgCl_2$, pH 6.0, dialyzed against TBS, and further purified by performing gel filtration chromatography on a Superdex 200 16/60 column equilibrated with TBS.

Structural analysis of NZ-1 with and without bound PA peptide

The purified NZ-1 Fab was concentrated to ∼10 mg/ml by ultrafiltration using Spin-X UF (MWCO: 10,000) and subjected to the crystallization trials. Initial screening of crystallization conditions was carried out using Crystal Screen 1 and 2 (Hampton Research) by using the sitting drop vapor-diffusion method, resulting in many hit conditions. Upon the optimization, the diffraction quality crystals were grown under the condition of 0.1 M sodium citrate buffer, pH 5.6, and 12–15% (w/v) PEG4000. Crystals were cryoprotected with the same buffer containing 10% (v/v) glycerol and used for data collection at BL17A of Photon Factory (Tsukuba, Japan) and BL15A1 of The National Synchrotron Radiation Research Center (NSRRC, Hsinchu, Taiwan). As the data sets collected at two beamlines have the same crystal system (Table 1), these data were combined and processed using the HKL2000 program package (Otwinowski and Minor, 1997). Initial phases were determined by using the molecular replacement method using a rat anti-NGF AD11 antibody Fab (IgG2a) structure (Protein Data Bank ID: 1ZAN) as a search model, by the Phaser-MR (Mccoy et al., 2007) program. For the determination of the NZ-1–PA14 complex structure, NZ-1 Fab was mixed with the PA14 peptide at a molar ratio of 1:3 and subjected to the crystallization process. A diffraction quality co-crystal was grown under the condition of 0.1 M sodium citrate buffer, pH 5.6, and 24% (w/v) PEG4000, cryoprotected with 10% (v/v) ethylene glycol in the same buffer, and an X-ray diffraction data set was collected at the beam line BL1A of Photon Factory. The data were processed using XDS program package (Kabsch, 2010). Initial phases were determined by using molecular replacement with the NZ-1 Fab structure described above as a search model. The structural models were built using COOT software (Emsley et al., 2010) with model refinement cycle with REFMAC5 (Murshudov et al., 2011) and phenix.refine (Adams et al., 2010) programs. The models were validated using the program MOLPROBITY (Chen et al., 2010). Data collection and refinement statistics are listed in Table 1. The interaction between the PA14 peptide and the NZ-1 Fab was analyzed using the program LIGPLOT (Wallace et al., 1995). All structural figures were prepared with the program PyMOL (Schrödinger, LLC).

Generation of DNA constructs

cDNAs encoding human α_6- and β_1-integrin chains were truncated after residues 612 and 481, respectively, to express a $\alpha_6\beta_1$-integrin headpiece fragment. The 12-residue PA-tag sequence was inserted into a site shown in Fig. 2A by performing overlap extension PCR. Similarly, PA-tagged version of mouse Sema3A was constructed from mouse full-length Sema3A cDNA N-terminally tagged with hexahistidine residues. The design of secreted the ectodomain fragment of integrin $\alpha_{IIb}\beta_3$ was conducted by adopting the strategy used for $\alpha_V\beta_3$ integrin, described previously (Takagi et al., 2002). Briefly, ACID and BASE peptides were appended at the C-termini of the complete ectodomain of human α_{IIb}- (residues 1–963) and β_3-integrin (residues 1–692) chains, resulting in the formation of a disulfide-linked α-helical coiled-coil knot called 'velcro' (O'shea et al., 1993). The PA-tag sequence was inserted at various sites of the α_{IIb} subunit, as shown in Fig. 3C. Each insertion position was designated based on the location in the domain and secondary structure elements defined by Xiao et al. (2004). For the cell surface expression of these integrins, mutated regions were introduced into the vectors coding for full-length α_{IIb} and β_3 subunits, as described previously (Luo et al., 2004). For the design of the 'activation-reporter' construct for mouse integrin β_1, the PA tag was inserted into the E-F loop of the hybrid domain of the mouse full-length expression construct.

The homology models of human $\alpha_6\beta_1$-integrin (Fig. 2A) and mouse $\alpha_4\beta_1$-integrin (Fig. 7A) headpiece fragments were built by using the program MODELLER (Eswar et al., 2008), using the structure of the $\alpha_5\beta_1$-integrin headpiece (Protein Data Bank ID: 3VI3) (Nagae et al., 2012) as a template.

Expression and immunoprecipitation of the soluble $\alpha_{IIb}\beta_3$ integrin

For the expression of soluble ectodomain fragments of $\alpha_{IIb}\beta_3$ integrin, HEK293T cells that had been plated on 6-well plates were transiently transfected with plasmid DNAs coding for soluble α_{IIb} and β_3 subunits (2 µg/subunit/well) using X-tremeGENE HP DNA Transfection Reagent (Roche). Culture supernatants were harvested ∼72 h after the transfection and incubated with either 2H11–Sepharose or NZ-1–Sepharose for ∼2 h at 4°C. After washing three times with TBS containing 1 mM $CaCl_2$ and 1 mM $MgCl_2$, the resin-bound $\alpha_{IIb}\beta_3$ integrin was eluted by using ×2 SDS sample buffer, subjected to 7.5% SDS-PAGE and stained with Oriole fluorescent dye (Bio-Rad). For some experiments, integrins were immunoprecipitated from the culture supernatants with purified IgG (anti-β3-integrin antibody 7E3, 2 µg/ml; anti-PA-tag antibody NZ-1, 2 µg/ml; anti-FLAG antibody M2, 2 µg/ml; and anti-Myc antibody 9E10, 2 µg/ml) and immobilized Protein G (GE Healthcare), followed by western blotting using biotinylated anti-velcro polyclonal antibody. For the detection, membranes were incubated with streptavidin conjugated to horseradish peroxidase (HRP) (VECTOR), developed with ECL™ Prime reagent, and analyzed using ImageQuant LAS 4000mini (GE Healthcare). Expression and immunoprecipitation of the $\alpha_6\beta_1$-integrin headpiece and Sema3A were performed with similar protocols, with the exception of using HEK293S GnT1 cells for $\alpha_6\beta_1$ integrin. As the positive control experiment for the immunoprecipitation, either GoH3–Sepharose (for $\alpha_6\beta_1$ integrin) or Ni-NTA agarose (for His_6–Sema3A) were used.

Biolayer interferometry

For the large-scale production of soluble $\alpha_{IIb}\beta_3$ integrin, transient transfection of Expi293F cells (Life Technologies) using ExpiFectamine 293 Transfection Kit (Life Technologies) was utilized. Briefly, 20-ml cell cultures were transfected with 13.3 µg each of DNAs coding for various PA-tagged α_{IIb}-integrin and wild-type β_3-integrin chains, and the culture medium was collected after 96 h. Each mutant integrin was purified with NZ-1–Sepharose column chromatography, followed by further gel filtration purification on a Superdex 200 10/300 GL column. After concentration to ∼0.7 mg/ml, these PA-bearing integrins were subjected to binding evaluation with BLI using Octet RED system (Pall ForteBio), as described previously (Fujii et al., 2014). Binding curves were analyzed with Octet Data Analysis software (Pall ForteBio) and curve-fitting using a 1:1 binding model.

Establishment of podoplanin-knockout cell line

A CRISPR/Cas plasmid (Sigma-Aldrich), which targets the sequence 5′-GACACTGAGACTACAGGTTTGG-3′ of human podoplanin, was transfected into HEK293T cells using a Gene Pulser Xcell electroporation system (Bio-Rad Laboratories). Single-cell cloning was performed by limiting dilution in 96-well plates using 10% FBS in Dulbecco's modified Eagle's medium (DMEM), and podoplanin expression was checked with flow cytometry using NZ-1. The transfection–cloning cycles were repeated until a complete lack of NZ-1 reactivity was attained. The stable nature of the knockout phenotype was confirmed by the lack of NZ-1 reactivity after more than ten passages. The established podoplanin-knockout cell line (293T-PA$^-$) showed similar morphology to that of the parent HEK293T cells both under a microscope and in the flow cytometry analysis (i.e. forward- and side- scattering characteristics), but exhibited some phenotypic differences, including a slight reduction in the growth rate (doubling time of ∼17 h) and a reduced (by ∼50%) level of protein secretion after transient transfection. These variations, however, can be seen among different laboratory strains of HEK293T cells, and it is unclear whether any of the changes are caused by podoplanin depletion.

Expression and flow cytometry analyses of full-length integrins on the cell surface

Transient transfection of full-length $\alpha_{IIb}\beta_3$-integrin into 293T-PA$^-$ cells was conducted under the same conditions utilized for the soluble ectodomain fragments described above. Cells were harvested after ∼48 h of transfection, washed twice with fresh serum-containing medium and resuspended in Tyrode's buffer (137 mM NaCl, 12 mM $NaHCO_3$, 2.6 mM KCl, 5 mM HEPES, 2 mM $CaCl_2$, 2 mM $MgCl_2$, 1 mg/ml BSA, 1 mg/ml dextrose, pH 7.4). For the integrin expression analysis, cells were incubated with the 10E5 antibody (1 µg/ml) and NZ-1 (0.5 µg/ml) for 30 min at 20°C, followed by staining with Alexa-Fluor-488-conjugated goat anti-mouse IgG (1:400) and phycoerythrin-conjugated goat anti-rat IgG polyclonal antibody (1:1000). Flow cytometry was performed on an EC800 system (SONY), and the data were analyzed with FlowJo software (Tomy Digital Biology). For the evaluation of epitope exposure, cells were incubated with a mixture of DyLight680-conjugated AP3 (5 µg/ml) and FITC-conjugated NZ-1 (0.5 µg/ml) antibodies in the absence or presence of the activation mixture, comprising 0.5 mM $MnCl_2$ and 1 mM RGD peptide. Evaluation of the LIBS exposure on mouse β_1 integrin was performed in a similar way, using the 293T-PA$^-$ cells transiently transfected with human α_4 integrin and mouse β_1 integrin. Cells were incubated with the NZ-1 (1 µg/ml) or 9EG7 (5 µg/ml) antibodies for 30 min at 20°C, followed by staining with the Alexa-Fluor-488-conjugated goat anti-rat IgG polyclonal antibody (1:400).

Ligand-binding assay for cell surface $\alpha_{IIb}\beta_3$

The ligand-binding activity of $\alpha_{IIb}\beta_3$ integrin on the cell surface was evaluated by the flow cytometry analysis of PAC-1 binding. PAC-1 is a ligand-mimetic anti-$\alpha_{IIb}\beta_3$-integrin antibody whose binding is solely dependent on the high-affinity state of integrin, serving as a surrogate for the physiological ligand fibrinogen (Tomiyama et al., 1992). The 293T-PA$^-$ cells that had been transiently transfected with various full-length $\alpha_{IIb}\beta_3$-integrin constructs were incubated with Tyrode's buffer containing FITC–PAC-1 (1:20 dilution) and DyLight680-AP3 (5 µg/ml) for 30 min at 20°C, washed once and resuspended in Tyrode's buffer, and analyzed on an EC800 flow cytometer. When activation of the integrin was required, cells were incubated with 15 mM dithiothreitol (DTT) for 10 min at 37°C, which is known to activate resting (i.e. low affinity) $\alpha_{IIb}\beta_3$ integrin (Kouns et al., 1994).

Acknowledgements

We would like to thank the staff of the beamlines at Photon Factory and National Synchrotron Radiation Research Center for their help with X-ray data collection; Emiko Mihara and Keiko Tamura-Kawakami for excellent technical assistance; and Mie Sakai for preparation of the manuscript.

Competing interests

The authors declare no competing or financial interests.

Author contributions

Y.F. and Y.M. designed and performed experiments, and wrote the manuscript. T.A., Y.K., S.O. and M.K.K. performed experiments and analyzed the data. Y.K. supervised the experiments and analyzed the data. J.T. conceived the experimental design, analyzed the data and wrote the manuscript. All authors contributed to the preparation of the manuscript.

Funding

This work was supported in part by the Grant-in-Aid for Scientific Research on Innovative Areas (Analysis and Synthesis of Multidimensional Immune Organ Network to J.T.) from the Ministry of Education, Culture, Sports, Science and Technology of Japan (MEXT); by the 'Platform for Drug Discovery, Informatics, and Structural Life Science' grant from the MEXT; by the Japan Agency for Medical Research and Development (AMED) (to J.T. and Y.K.); by the 'X-ray Free Electron Laser Priority Strategy Program' grant (to J.T.) from the MEXT; by the Basic Science and Platform Technology Program for Innovative Biological Medicine from the MEXT and AMED (to Y.K.); and by the Regional Innovation Strategy Support Program from the MEXT (to Y.K.).

Data availability

Atomic coordinates and structural factors have been deposited in the Protein Data Bank under accession numbers 4YNY (ligand-free NZ-1 Fab) and 4YO0 (NZ-1 Fab in complex with the PA14 peptide).

Supplementary information

Supplementary information available online at
http://jcs.biologists.org/lookup/suppl/doi:10.1242/jcs.176685/-/DC1

References

Adams, P. D., Afonine, P. V., Bunkóczi, G., Chen, V. B., Davis, I. W., Echols, N., Headd, J. J., Hung, L.-W., Kapral, G. J., Grosse-Kunstleve, R. W. et al. (2010). PHENIX: a comprehensive Python-based system for macromolecular structure solution. *Acta Crystallogr. D Biol. Crystallogr.* **66**, 213-221.

Bazzoni, G., Shih, D.-T., Buck, C. A. and Hemler, M. E. (1995). Monoclonal antibody 9eg7 defines a novel beta(1) integrin epitope induced by soluble ligand and manganese, but inhibited by calcium. *J. Biol. Chem.* **270**, 25570-25577.

Carman, C. V. and Springer, T. A. (2003). Integrin avidity regulation: are changes in affinity and conformation underemphasized? *Curr. Opin. Cell Biol.* **15**, 547-556.

Chang, H. C., Bao, Z., Yao, Y., Tse, A. G., Goyarts, E. C., Madsen, M., Kawasaki, E., Brauer, P. P., Sacchettini, J. C., Nathenson, S. G. et al. (1994). A general method for facilitating heterodimeric pairing between two proteins: application to expression of alpha and beta T-cell receptor extracellular segments. *Proc. Natl. Acad. Sci. USA* **91**, 11408-11412.

Chen, V. B., Arendall, W. B., Headd, J. J., Keedy, D. A., Immormino, R. M., Kapral, G. J., Murray, L. W., Richardson, J. S. and Richardson, D. C. (2010). MolProbity: all-atom structure validation for macromolecular crystallography. *Acta Crystallogr. D Biol. Crystallogr.* **66**, 12-21.

Coller, B. S. (1985). A new murine monoclonal antibody reports an activation-dependent change in the conformation and/or microenvironment of the platelet glycoprotein IIb/IIIa complex. *J. Clin. Invest.* **76**, 101-108.

Dennison, S. M., Anasti, K. M., Jaeger, F. H., Stewart, S. M., Pollara, J., Liu, P., Kunz, E. L., Zhang, R., Vandergrift, N., Permar, S. et al. (2014). Vaccine-induced HIV-1 envelope gp120 constant region 1-specific antibodies expose a CD4-inducible epitope and block the interaction of HIV-1 gp140 with galactosylceramide. *J. Virol.* **88**, 9406-9417.

Dinculescu, A., McDowell, J. H., Amici, S. A., Dugger, D. R., Richards, N., Hargrave, P. A. and Smith, W. C. (2002). Insertional mutagenesis and immunochemical analysis of visual arrestin interaction with rhodopsin. *J. Biol. Chem.* **277**, 11703-11708.

Dyson, H. J., Lerner, R. A. and Wright, P. E. (1988). The physical basis for induction of protein-reactive antipeptide antibodies. *Annu. Rev. Biophys. Biophys. Chem.* **17**, 305-324.

Emsley, P., Lohkamp, B., Scott, W. G. and Cowtan, K. (2010). Features and development of Coot. *Acta Crystallogr. D Biol. Crystallogr.* **66**, 486-501.

Eswar, N., Eramian, D., Webb, B., Shen, M.-Y. and Sali, A. (2008). Protein structure modeling with MODELLER. *Methods Mol. Biol.* **426**, 145-159.

Facey, S. J. and Kuhn, A. (2003). The sensor protein KdpD inserts into the Escherichia coli membrane independent of the Sec translocase and YidC. *Eur. J. Biochem.* **270**, 1724-1734.

Fujii, Y., Kaneko, M., Neyazaki, M., Nogi, T., Kato, Y. and Takagi, J. (2014). PA tag: a versatile protein tagging system using a super high affinity antibody against a dodecapeptide derived from human podoplanin. *Protein Expres Purif.* **95**, 240-247.

Guruprasad, K. and Rajkumar, S. (2000). Beta-and gamma-turns in proteins revisited: a new set of amino acid turn-type dependent positional preferences and potentials. *J. Biosci.* **25**, 143-156.

Humphries, M. J. (2004). Monoclonal antibodies as probes of integrin priming and activation. *Biochem. Soc. Trans.* **32**, 407-411.

Humphries, M. J., Symonds, E. J. and Mould, A. P. (2003). Mapping functional residues onto integrin crystal structures. *Curr. Opin. Struct. Biol.* **13**, 236-243.

Irannejad, R., Tomshine, J. C., Tomshine, J. R., Chevalier, M., Mahoney, J. P., Steyaert, J., Rasmussen, S. G. F., Sunahara, R. K., El-Samad, H., Huang, B. et al. (2013). Conformational biosensors reveal GPCR signalling from endosomes. *Nature* **495**, 534-538.

Johnson, J. L., Entzminger, K. C., Hyun, J., Kalyoncu, S., Heaner, D. P., Jr, Morales, I. A., Sheppard, A., Gumbart, J. C., Maynard, J. A. and Lieberman, R. L. (2015). Structural and biophysical characterization of an epitope-specific engineered Fab fragment and complexation with membrane proteins: implications for co-crystallization. *Acta Crystallogr. D Biol. Crystallogr.* **71**, 896-906.

Kabsch, W. (2010). Xds. *Acta Crystallogr. D Biol. Crystallogr.* **66**, 125-132.

Kendall, R. T. and Senogles, S. E. (2006). Investigation of the alternatively spliced insert region of the D2L dopamine receptor by epitope substitution. *Neurosci. Lett.* **393**, 155-159.

Koide, S. (2009). Engineering of recombinant crystallization chaperones. *Curr. Opin. Struct. Biol.* **19**, 449-457.

Kouns, W. C., Steiner, B., Kunicki, T. J., Moog, S., Jutzi, J., Jennings, L. K., Cazenave, J. P. and Lanza, F. (1994). Activation of the fibrinogen binding site on platelets isolated from a patient with the Strasbourg I variant of Glanzmann's thrombasthenia. *Blood* **84**, 1108-1115.

Krauss, N., Wessner, H., Welfle, K., Welfle, H., Scholz, C., Seifert, M., Zubow, K., Aÿ, J., Hahn, M., Scheerer, P. et al. (2008). The structure of the anti-c-myc antibody 9E10 Fab fragment/epitope peptide complex reveals a novel binding mode dominated by the heavy chain hypervariable loops. *Proteins* **73**, 552-565.

Luo, B.-H., Springer, T. A. and Takagi, J. (2004). A specific interface between integrin transmembrane helices and affinity for ligand. *PLoS Biol.* **2**, e153.

McCoy, A. J., Grosse-Kunstleve, R. W., Adams, P. D., Winn, M. D., Storoni, L. C. and Read, R. J. (2007). Phaser crystallographic software. *J. Appl. Crystallogr.* **40**, 658-674.

Mitchell, W. B., Li, J. H., Singh, F., Michelson, A. D., Bussel, J., Coller, B. S. and French, D. L. (2003). Two novel mutations in the alpha IIb calcium-binding domains identify hydrophobic regions essential for alpha IIbbeta 3 biogenesis. *Blood* **101**, 2268-2276.

Morlacchi, S., Sciandra, F., Bigotti, M. G., Bozzi, M., Hübner, W., Galtieri, A., Giardina, B. and Brancaccio, A. (2012). Insertion of a myc-tag within alpha-dystroglycan domains improves its biochemical and microscopic detection. *BMC Biochem.* **13**, 14.

Mould, A. P., Barton, S. J., Askari, J. A., McEwan, P. A., Buckley, P. A., Craig, S. E. and Humphries, M. J. (2003). Conformational changes in the integrin beta A domain provide a mechanism for signal transduction via hybrid domain movement. *J. Biol. Chem.* **278**, 17028-17035.

Murshudov, G. N., Skubák, P., Lebedev, A. A., Pannu, N. S., Steiner, R. A., Nicholls, R. A., Winn, M. D., Long, F. and Vagin, A. A. (2011). REFMAC 5 for the refinement of macromolecular crystal structures. *Acta Crystallogr. D Biol. Crystallogr.* **67**, 355-367.

Nagae, M., Re, S., Mihara, E., Nogi, T., Sugita, Y. and Takagi, J. (2012). Crystal structure of alpha5beta1 integrin ectodomain: atomic details of the fibronectin receptor. *J. Cell Biol.* **197**, 131-140.

Newman, P. J., Allen, R. W., Kahn, R. A. and Kunicki, T. J. (1985). Quantitation of membrane glycoprotein IIIa on intact human platelets using the monoclonal antibody, AP-3. *Blood* **65**, 227-232.

O'shea, E. K., Lumb, K. J. and Kim, P. S. (1993). Peptide Velcro - design of a heterodimeric coiled coil. *Curr. Biol.* **3**, 658-667.

Otwinowski, Z. and Minor, W. (1997). Processing of X-ray diffraction data collected in oscillation mode. *Methods Enzymol.* **276**, 307-326.

Peerschke, E. I. and Coller, B. S. (1984). A murine monoclonal antibody that blocks fibrinogen binding to normal platelets also inhibits fibrinogen interactions with chymotrypsin-treated platelets. *Blood* **64**, 59-63.

Smith, W. C., Dinculescu, A., Peterson, J. J. and McDowell, J. H. (2004). The surface of visual arrestin that binds to rhodopsin. *Mol. Vis.* **10**, 392-398.

Spangler, B. D. (1991). Binding to native proteins by antipeptide monoclonal antibodies. *J. Immunol.* **146**, 1591-1595.

Springer, T. A. (1998). An extracellular beta-propeller module predicted in lipoprotein and scavenger receptors, tyrosine kinases, epidermal growth factor precursor, and extracellular matrix components. *J. Mol. Biol.* **283**, 837-862.

Tainer, J. A., Getzoff, E. D., Alexander, H., Houghten, R. A., Olson, A. J., Lerner, R. A. and Hendrickson, W. A. (1984). The reactivity of anti-peptide antibodies is a function of the atomic mobility of sites in a protein. *Nature* **312**, 127-134.

Takagi, J. and Springer, T. A. (2002). Integrin activation and structural rearrangement. *Immunol. Rev.* **186**, 141-163.

Takagi, J., Isobe, T., Takada, Y. and Saito, Y. (1997). Structural interlock between ligand-binding site and stalk-like region of beta1 integrin revealed by a monoclonal antibody recognizing conformation-dependent epitope. *J. Biochem.* **121**, 914-921.

Takagi, J., Erickson, H. P. and Springer, T. A. (2001). C-terminal opening mimics "inside-out" activation of integrin a5b1. *Nat. Struct. Biol.* **8**, 412-416.

Takagi, J., Petre, B. M., Walz, T. and Springer, T. A. (2002). Global conformational rearrangements in integrin extracellular domains in outside-in and inside-out signaling. *Cell* **110**, 599-611.

Tomiyama, Y., Brojer, E., Ruggeri, Z. M., Shattil, S. J., Smiltneck, J., Gorski, J., Kumar, A., Kieber-Emmons, T. and Kunicki, T. J. (1992). A molecular model of RGD ligands. Antibody D gene segments that direct specificity for the integrin alpha IIb beta 3. *J. Biol. Chem.* **267**, 18085-18092.

Walker, F., Orchard, S. G., Jorissen, R. N., Hall, N. E., Zhang, H.-H., Hoyne, P. A., Adams, T. E., Johns, T. G., Ward, C., Garrett, T. P. et al. (2004). CR1/CR2 interactions modulate the functions of the cell surface epidermal growth factor receptor. *J. Biol. Chem.* **279**, 22387-22398.

Wallace, A. C., Laskowski, R. A. and Thornton, J. M. (1995). LIGPLOT: a program to generate schematic diagrams of protein-ligand interactions. *Protein Eng.* **8**, 127-134.

Wood, D. W. (2014). New trends and affinity tag designs for recombinant protein purification. *Curr. Opin. Struct. Biol.* **26**, 54-61.

Xiao, T., Takagi, J., Coller, B. S., Wang, J.-H. and Springer, T. A. (2004). Structural basis for allostery in integrins and binding to fibrinogen-mimetic therapeutics. *Nature* **432**, 59-67.

Zhu, J., Luo, B.-H., Xiao, T., Zhang, C., Nishida, N. and Springer, T. A. (2008). Structure of a complete integrin ectodomain in a physiologic resting state and activation and deactivation by applied forces. *Mol. Cell* **32**, 849-861.